Paper Number: IWSH2025-083

The 13th International Workshop on Ship and Marine Hydrodynamics
Fukuoka, Japan, August 25 - 28, 2025

Comparison of Approaches for Parametric Sea State Estimation using the Wave-Buoy Analogy and Neural Networks on Full-Scale Measurement Data

Johanna Serr, Malwin Wermbter and Moustafa Abdel-Maksoud

Institute for Fluid Dynamics and Ship Theory, Technical University of Hamburg, Hamburg, Germany
Corresponding author: johanna.serr@tuhh.de

Abstract. Monitoring the surrounding sea state enhances operational safety and energy efficiency of vessels during voyage. The directional sea state can be estimated from measured vessel responses using physics-based models following the Wave-Buoy Analogy (WBA) or data-driven methods like Convolutional Neural Networks (CNNs). This study explores both approaches for parametric sea state estimation using simulation and full-scale measurement data of a barge. The issue of local minimum convergence in the least-squares algorithm is addressed by a modified implementation of the parametric WBA. The modification involves constraining the relative wave direction during optimization, leading to more robustness against outliers in the estimation of the peak period and relative wave direction. The study emphasizes that the methods provide feasible approaches for parametric sea state estimation on the given data, with the WBA requiring knowledge of the vessel-specific conditions and the CNN depending on the representativeness of the training data.

Keywords: Sea state estimation, wave-buoy analogy, neural networks, full-scale measurements, response amplitude operators

1 Introduction

The accurate estimation of sea state parameters such as wave height, period and direction is critical for mariners for enhancing operational safety [1] as well as navigational efficiency [2]. Commonly, the sea state can be obtained from fixed buoys, weather data bases or wave radars. They, however, can lack real-time, location-specific data and in case of radar systems be cost-intensive [3]. In contrast, the Wave-Buoy Analogy (WBA) and Machine Learning (ML) models utilize vessel acceleration measurements to estimate the surrounding sea state conditions and offer a reliable and cost-efficient alternative to traditional measuring methods.

The WBA as described by Iseki and Ohtsu [4] or Tannuri et al. [3] is a physics-based model in frequency domain that assumes linear relations between wave excitation and vessel responses. The WBA is limited by (i) the constrains to mild or moderate sea state conditions due to the linear theory (ii) the dependence on the quality of the RAOs which include the knowledge of the operational conditions as well as the geometry of the vessel and (iii) the influence of the vessel as low-pass filter, which causes the excitation of high-frequency waves to be attenuated. One distinguishes between parametric [3] and non-parametric approaches [4], which yield in either estimating the statistical parameters of an assumed spectral form or in the non-parameterized spectrum. Advantages and disadvantages of both approaches have been discussed by Tannuri et al. [3] as well as Nielsen [5]. In case of parametric modeling, the discrepancy between measured and computed vessel responses can be minimized using genetic optimization or gradient search algorithms [6]. Non-linear optimization techniques such as the least squares method, however, minimize problems that are not globally convex to a local minimum, which has been proven to affect the accuracy of the parametric WBA [5]. Pascoal et al. [7] suggest instead using global search techniques or performing tests regarding the relative wave direction in a post-processing step. Furthermore, studies have shown that the estimated distribution of the wave energy is influenced by the filtering effect of the vessel [8] as well as the short-term variability of the relative phase angle between the ship responses [9].

In addition to model-based approaches, data-driven models like Machine Learning (ML) are used for sea state estimation. The major advantage of ML is its capability to develop non-linear models based on a

data set while having close-to real-time execution. Mittendorf et al. [10] performed a comparison of multiple neural networks for sea state estimation in time and frequency domain. In another study, the authors concluded that the estimation of the wave direction is more complex than estimating the wave height and peak period [11]. Kawai et al. [12] applied a Convolutional Neural Network (CNN) in order to estimate the statistical parameters of the Ochi-Hubble spectrum on measurement data. They show that compared to the wave height, frequency and kurtosis, the estimation accuracy of the wave direction varies the largest. Han et al. [13] describe how due to the ML models inability to extrapolate outside of the training data, these models are likely to fail in sea state conditions that were not included in the training data. As the physics-based and the data-driven methods have shown complementary advantages and disadvantages, latest research has spurred into the development of hybrid models that combine WBA and ML models [13,14].

This study aims at investigating the capabilities of the WBA and a CNN on simulation as well as full-scale measurement data of a barge. The WBA was implemented using the least-squares algorithm and the influence of the optimization to local minima is investigated. A modified implementation of the WBA is presented, which bounds the least-squares algorithm to a plausible range of wave directions. The study is organised as follows: Section 2 is devoted to the methodology which comprises the theory of the WBA as well as a brief introduction to neural networks. Details of the vessel and the description of the data are given in Section 3. The results are presented in Section 4, followed by the discussion in Section 5 and the conclusions in Section 6.

2 Methodology

2.1 Parametric Modeling of the Wave-Buoy Analogy

Detailed descriptions of the theory and the governing equations of the WBA are given by Iseki and Ohtsu [4] as well as Nielsen et al. [15]. Based on the assumptions that linearity exists between incident waves and vessel responses and that the sea state behaves stationary and ergodic, the cross spectrum

$$S_{ij}(\omega_e) = \int_{-\pi}^{\pi} \Phi_i(\omega_e, \mu)\, \overline{\Phi_j(\omega_e, \mu)}\, E(\omega_e, \mu)\, \mathrm{d}\mu \tag{1}$$

between the i-th and j-th motion responses of encounter frequency ω_e can be determined using the directional wave spectrum $E(\omega_e, \mu)$ and the complex-valued transfer functions $\Phi_{i,j}(\omega_e, \mu)$, with the bar denoting the complex conjugate. The angle μ depicts the relative wave direction, which in this study is defined as 0° for following seas, 90° for starboard beam, 180° for head sea and 270° for port beam. The equation is conveniently formulated in absolute frequency domain, which requires the mapping of the encounter frequency

$$\omega_\mathrm{e} = \omega - \omega^2 \frac{U}{g} \cos(\mu) \tag{2}$$

to absolute frequency ω using the ship forward speed U and gravitational acceleration g. The relationship given in Eq. 2 is non-unique in cases of beam, quartering and following sea resulting in the triple-value function problem, as addressed by Iseki and Ohtsu [4]. When regarding multiple degrees of freedom, a system of equations can be obtained from Eq. 1, whose solution can be approximated through minimizing

$$\min\chi^2 \equiv \min\|\mathbf{A}\mathbf{f}(\mathbf{x}) - \mathbf{b}\|^2 \tag{3}$$

using the least squares method with L_2 norm. In the equation, $\mathbf{b}$ represents the measured responses, $\mathbf{A}$ holds the components of the transfer functions and $\mathbf{f}(\mathbf{x})$ is a function expressing the wave spectrum depending on sea state parameters $\mathbf{x}$. In order to equally weight the magnitudes of measured responses, the response spectra are normalized to a maximal absolute value of 1. The transfer functions are normalized accordingly.

2.2 Bounded WBA

The modification of the WBA implementation as described above aims at preventing the least-squares algorithm to converge to a local minimum by constraining the estimation of the relative wave direction μ. The procedure is based on studies by Brodtkorb and Nielsen [16], who distinguish between waves coming from

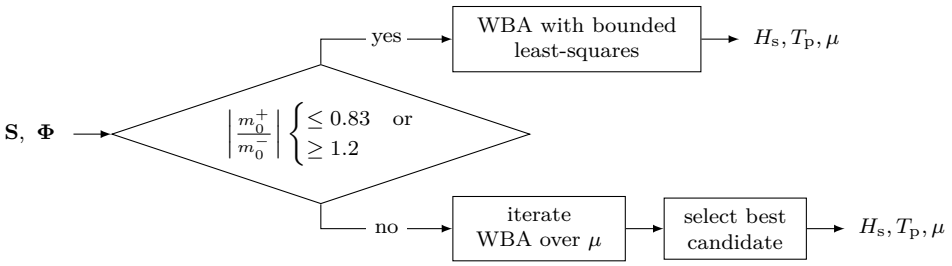

Fig. 1. Algorithm of the bounded WBA.

port and starboard using the imaginary part of the heave-roll cross spectum $\mathrm{Im}\{S_{34}\}$ and between head and following sea using the imaginary part of the heave-pitch cross spectum $\mathrm{Im}\{S_{35}\}$. For this purpose, the zeroth-order moment

$$m_0 = \int_0^\infty S(\omega_\mathrm{e})\,\mathrm{d}\omega_\mathrm{e} \tag{4}$$

is calculated for $\mathrm{Im}\{S_{34}\}$ and $\mathrm{Im}\{S_{35}\}$. The case distinction is executed based on the sign of m_0 following

$$m_0\big(\,\mathrm{Im}\{S_{34}\}\big) = \textstyle\int_0^\infty \mathrm{Im}\{S_{34}\}\,\mathrm{d}\omega_\mathrm{e} \begin{cases} < 0 & \mu \in [\ \ 0°,\,\ldots,\,180°) \\ \geq 0 & \mu \in [180°,\,\ldots,\,360°) \end{cases} \tag{5}$$

$$m_0\big(\,\mathrm{Im}\{S_{35}\}\big) = \textstyle\int_0^\infty \mathrm{Im}\{S_{35}\}\,\mathrm{d}\omega_\mathrm{e} \begin{cases} < 0 & \mu \in [\ \ 0°,\,\ldots,\,90°) \cup [270°,\,\ldots,\,360°) \\ \geq 0 & \mu \in [\ 90°,\,\ldots,\,270°)\,. \end{cases} \tag{6}$$

The algorithm is illustrated in Fig. 1. First, $m_0\big(\,\mathrm{Im}\{S_{ij}\}\big)$ of the measured responses for $ij = [(3,4),(3,5)]$ are checked for ambiguity. This is done by comparing the integrals over the positive values of $\mathrm{Im}\{S_{ij}\}$, m_0^+, and negative values m_0^-. The case distinction as defined above is set as trustworthy if either m_0^+ or m_0^- predominates such that

$$\left|\frac{m_0^+\big(\,\mathrm{Im}\{S_{ij}\}\big)}{m_0^-\big(\,\mathrm{Im}\{S_{ij}\}\big)}\right| \begin{cases} \leq 0.83 & \text{or} \\ \geq 1.2\,. \end{cases} \tag{7}$$

If the condition is satisfied, the least-squares algorithm is solved with bounds for μ according to Eq. 5 and 6. Otherwise, the WBA is executed by iterating over the range of angles from 0° to 360° in steps of 10°. Hereby, the relative wave direction is set as fixed parameter and only the significant wave height and the peak period are optimized by the algorithm. From the 36 results, the sea state parameters yielding the lowest residual are selected as final estimation.

2.3 Artificial Neural Networks

The concept of neural networks was first introduced by Rosenblatt [17] and the theoretical background is given by Goodfellow et al. [18]. In supervised training, the main idea of artificial neural networks is to tune parameters of a given network architecture such that they replicate a function $g : \mathbf{x} \to \mathbf{y}$ mapping input $\mathbf{x}$ (features) and related output $\mathbf{y}$ (labels) of a training data set $\boldsymbol{\mathcal{D}} = \big\{\mathcal{D}_i = \big(\mathbf{x}, \mathbf{y}\big)_i,\ i = 1, 2, \ldots, N\big\}$ comprising N samples. The most basic neural network is a single neuron

$$\mathbf{y} = g(\mathbf{x}) \approx f(\mathbf{w},\ \mathbf{x}) = f\Big(\mathrm{bias} + \sum_{i=1}^{N} w_i x_i\Big)\,, \tag{8}$$

which approximates the function g by an activation function f, weights $\mathbf{w}$ and a bias parameter. The more neurons are arranged in consecutively manner, the more trainable parameters are added to the network such that

$$\mathbf{y} \approx f_L\Big(\mathrm{bias}_L, \mathbf{w}_L, f_{L-1}\big(\mathrm{bias}_{L-1}, \mathbf{w}_{L-1},\ \ldots,\ f_1(\mathrm{bias}_1, \mathbf{w}_1, \mathbf{x})\big)\Big)\,, \tag{9}$$

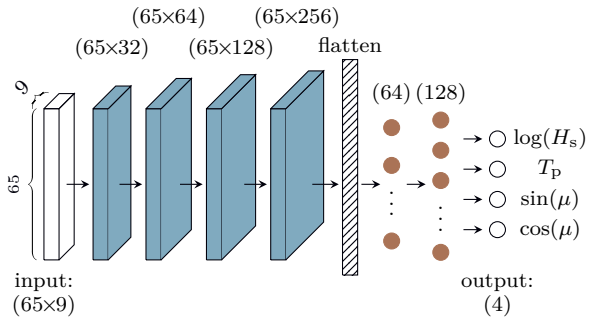

Fig. 2. Architecture of the CNN consisting of convolutional (blue), flatten (shaded) and fully-connected layers (red). The sizes of the layers are given. Cross spectral sequences of vessel responses serve as input and the output consists of the sea state parameters.

where L depicts the number of layers. A neural network is called feed-forward if the neurons are connected in unidirectional order towards the output layer and fully-connected if each layer is connected to every other neuron in the next layer. A common feed-forward architecture type is the Convolutional Neural Network (CNN), whose composition typically comprises a convolution part, pooling or flatten as well as fully-connected layers. In the process of convolution, features of interest are extracted from the data by using a kernel. In the process of training, the discrepancy between estimation and ground truth is measured by a loss function. The optimization is commonly carried out using gradient-descent and back-propagation methods.

The architecture of the proposed CNN is presented in Fig. 2. The network consists of four convolutional layers, a flatten layer and two fully-connected layers. The sizes of the layers were determined in a study of hyperparameters, which is described in Appendix A. Prior to the training, the logarithm was applied to the significant wave height H_s to enforce a more symmetrical shape on its data distribution [10]. The relative wave direction μ was split into its sine and cosine values in order to avoid its circular ambiguity. The features and labels were scaled to ranges between 0 and 1 following the Min-Max normalization. The mean squared error was applied as loss function and the tangens hyperbolicus as activation function with exception of the last layer, which holds no activation. The Adam optimizer was utilized with exponential learning rate starting at 10^{-5} and decay rate of 0.95.

3 Data Acquisition

The vessel investigated in this study is a barge with main particulars listed in Tab. 1. The barge is utilized for transporting containers between Pennsylvania and Puerto Rico. Measurements were conducted between July and November 2022 and the recorded GPS positions during data acquisition are depicted in Fig. 3. To mitigate the effects of shallow waters and refraction encountered in Delaware Bay, only data samples below a latitude threshold of 38° were considered. Next to the GPS position, the accelerations of the heave, pitch and roll motions were measured. After data processing, the total number of data samples came to 1213 with temporal length of 1 h. The vessel's forward speed U was derived from the processed GPS data, while sea state information was sourced from the Global Ocean Waves Reanalysis provided by the Copernicus Marine Service [19]. Fig. 3 presents the occurences of significant wave height, peak period and relative wave direction next to the vessel speed U. The significant wave height H_s approaches the shape of an exponential distribution with maximum observed value of 3.1 m, whereas the distribution of T_p is symmetrical with mean value of 8.4 s. In most cases, the relative wave direction corresponds to beam seas. The distribution of the vessel speed shows that the barge predominantly operates at $U = 5.2\,\mathrm{m/s}$, corresponding to a Froude number of $\mathrm{Fr} = U/\sqrt{g \cdot L_{pp}} \approx 0.15$. No information about the draught and center of gravity were recorded.

For training the neural network, a synthetic data set was generated by carrying out simulations of the barge using the impulse response method for ship motions based on the theory of Cummins [20]. Short-crested, irregular sea state is modeled by superposing elementary waves following linear wave theory with the JONSWAP spectrum selected as ocean wave spectrum. The equation of motion is solved in time domain using frequency-dependent hydrodynamic mass and damping coefficients, which were pre-calculated using

Table 1. Main particulars of the barge.

Parameter	Unit	Abbreviation	Value
Length between perpendiculars	[m]	L_{pp}	122
Breadth	[m]	B_{WL}	32.2
Design draught	[m]	T_{D}	5.16
Block coefficient	[-]	c_{B}	0.85

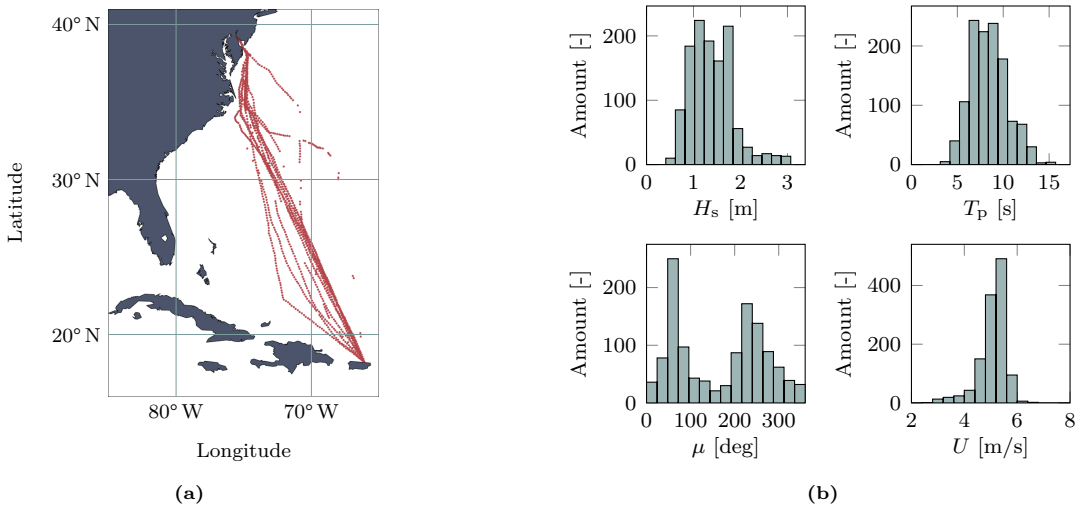

Fig. 3. Left: GPS positions of the barge for the period of data acquisition. Right: Occurrences of significant wave height H_{s}, peak period T_{p}, relative wave direction μ and forward speed of the vessel U during the measurements.

a frequency-domain panel method. For a more detailed description of the numerical model, the reader is referred to Wermbter and Maksoud [21]. In total, 5000 Jonswap spectra were generated for ratios between peak wave length to ship length $L_{\mathrm{p}}/L_{\mathrm{pp}} \in \{0.25, \ldots, 3.5\}$ and wave steepnesses $\pi H_{\mathrm{s}}/L_{\mathrm{p}} \in \{0.01, \ldots, 0.15\}$. The relative wave direction was varied randomly between 0° and 360°. The resulting joint distribution of H_{s} and T_{p} is given in Fig. 4, next to long-term sea state statistics as well as the sea state conditions encountered by the barge during the measurements. The simulated data set encompasses a larger range of wave heights and peak periods compared to the sea state statistics; however, this was intended in order to ensure that the applicability of the neural network also covers heavy seas, which are of special interest regarding ship safety. Furthermore, it can be observed that the measured occurrences of wave height and peak period are well represented within the simulation data. It is assumed that the barge mostly operated in similar loading conditions during the measurements. Therefore, only one operating point was included in the data set. The forward speed of the vessel was set to $U = 5.2\,\mathrm{m/s}$. As no information about the draught T as well as the vertical center of gravity VCG were given, the values had to be guessed and were set to $T = 3.84\,\mathrm{m}$ and $VCG = 9.6\,\mathrm{m}$. The length of one data sample is one hour for both the processed measurement data as well as the simulated data with time step size of 0.25 s. In order to transfer the vessel accelerations to frequency domain, the Welch algorithm is applied with a Hann window length of 512.

4 Results

4.1 Simulation data

The WBA and the bounded WBA, abbreviated bWBA in the following, were applied to the test set data of the CNN, c.f. Appendix A, with the results presented in Fig. 5. Next to the integral parameters, the peak period $T_{\mathrm{p}}^{\mathrm{e}}$ in encounter frequency domain is calculated according to Eq. 2 and will be part of the comparison.

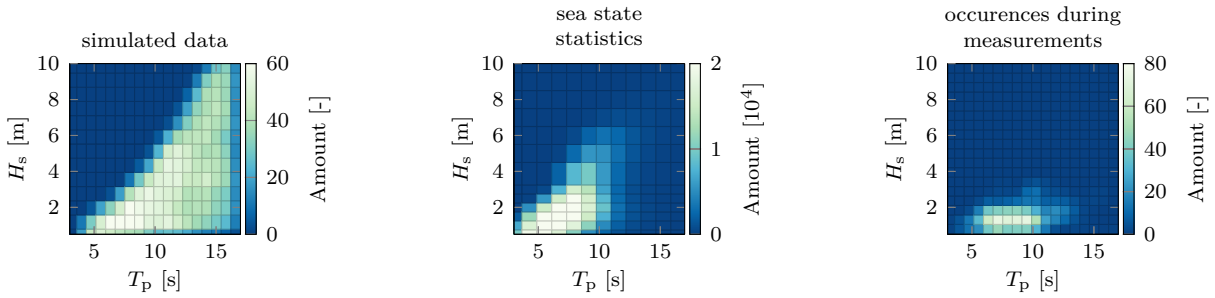

Fig. 4. Joint distribution of significant wave height H_s and peak period T_p in the simulated data (left), sea state statistics at the geographical position of 70°W of Longitude and 30° of Latitude [22] (middle) and the conducted measurements (right).

The mean normalized absolute error MNAE as well as the mean absolute error MAE

$$\text{MNAE} = \frac{1}{N}\sum_{i=1}^{N}\epsilon_i,\ \epsilon_i := \frac{|y_i - \hat{y}_i|}{y_i} \qquad \text{for } y \in [H_s,\ T_p,\ T_p^e]\,, \tag{10}$$

$$\text{MAE} \quad = \frac{1}{N}\sum_{i=1}^{N}\min\{|y_i - \hat{y}_i|, 360° - |y_i - \hat{y}_i|\} \qquad \text{for } y \in [\mu] \tag{11}$$

between ground truth y_i and estimation $\hat{y}_i$ are calculated for the corresponding sea state parameters. Starting with the WBA, the estimation of H_s shows the largest scatter as the absolute deviation between estimation and ground truth increases with higher values of H_s. The error in estimating the peak period T_p is low for most samples; however, in several cases the period is underestimated, with absolute errors reaching up to 10 s. A similar trend can be observed for the relative wave direction, where μ is estimated accurately most of the time with single outliers, resulting in a MAE = 34. In contrast to the latter two parameters, outliers are less prevalent in the determination of the encounter peak period T_p^e. When comparing the results of the bWBA to those of the WBA, the estimation accuracy increases for both the peak period and the relative wave direction. With the exception of a few samples, the majority of outliers were successfully mitigated. Due to these corrections, the estimation of T_p^e also slightly improves measured by the MNAE. The neural network yields the most accurate results when applied to this data set. Notably, the scatter of the significant wave height is reduced in comparison to the other two methods.

In the next step, the problem of convergence to local minima by the least-squares algorithm was investigated in more detail. The investigation is performed on two examples from the test set, which were previously estimated poorly by the WBA. The algorithm was adapted such that an iteration over the range of the relative wave direction in steps of 10° and over the peak period in steps of 0.7 s was carried out. Only the wave height H_s was treated as free parameter to be optimized by the least-squares algorithm. The aim of this study is to obtain a field of residuals in order to evaluate the inaccurate estimations of the WBA. The results are given in Fig. 6. The sea state parameters for Example 1 are $H_{s,1} = 3.9\,\text{m}$, $T_{p,1} = 14.5\,\text{s}$ and $\mu_1 = 310°$ and $H_{s,2} = 5.1\,\text{m}$, $T_{p,2} = 11.2\,\text{m}$, $\mu_2 = 236°$ for Example 2. The corresponding peak periods in encounter frequency domain are $T^e_{p,1} = 17.0\,\text{s}$ and $T^e_{p,2} = 9.6\,\text{s}$. In the first example, the problem exhibits a local minimum at the coordinate $(71°, 14.5\,\text{s})$ and a global minimum at $(310°, 14.5\,\text{s})$. The minima are nearly symmetrical regarding the wave direction with symmetry axis at 180°, resulting in an accurate estimation of the WBA for the peak period and an inaccurate estimation for the relative wave direction. In the second example, a local minimum is located at $(310°, 4.2\,\text{s})$ and no symmetry can be observed. In this case, the WBA estimates both the angle and the peak period incorrectly. Most notably, in both examples the estimations of the WBA and the bWBA for μ and T_p result in the same values of T_p^e.

4.2 Full-Scale Measurements

The uncertainty resulting from the unkown operating point and therefore unkown RAOs of the barge [23] is a substantial challenge in the evaluation of the measurement data. To address this, the effects of guessing

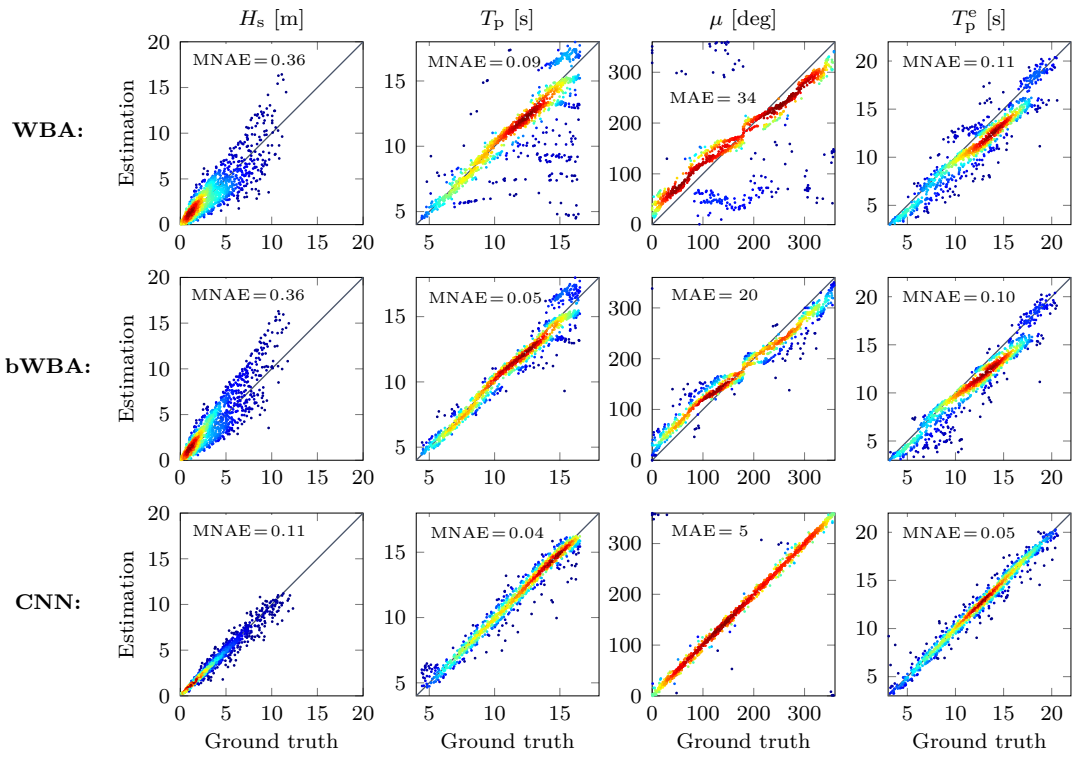

Fig. 5. Scatter density plots for sea state estimation of significant wave height H_s, peak period T_p, relative wave direction μ and peak period in encounter frequency domain T_p^e using the WBA (top), the bWBA (middle) and the CNN (bottom) on the simulated data set. Red dots indicate high and blue dots low density.

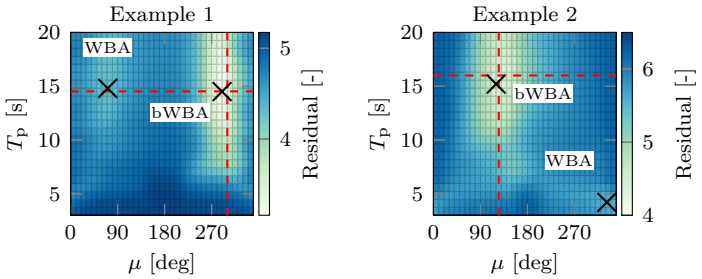

Fig. 6. Residuals showing local and global optima predicted by the WBA and bWBA, where lighter colors correspond to lower residual values and darker colors indicate higher residuals. The ground truth of μ and T_p is marked as red lines.

different values for draught T and the vertical center of gravity VCG on the estimation accuracy were investigated. The results of applying the bWBA for different combinations for T and VCG are presented in Fig. 7. The range of forward speed was discretised for Froude numbers $\mathrm{Fr} = [0.058, 0.116, 0.15]$. The estimation accuracy of the significant wave height is mainly influenced by the draught T, while the variation of VCG shows no substantial impact. The MNAE in estimating T_p is approximately the same for all parameter variations. The estimation of μ is influenced by both T and VCG and with increasing the both values, the MAE also increases. The combination of $T = 3.84\,\mathrm{m}$ and $VCG = 9.6\,\mathrm{m}$ results in the lowest deviation for all sea state parameters and was therefore selected for the final evaluation.

The final results are presented in Fig. 8 for all methods. The largest difference between the WBA and bWBA can be observed for the estimation of the relative wave direction, where outliers are corrected by the bWBA. Both methods exhibit the largest deviations for μ in cases of following seas. In terms of the peak

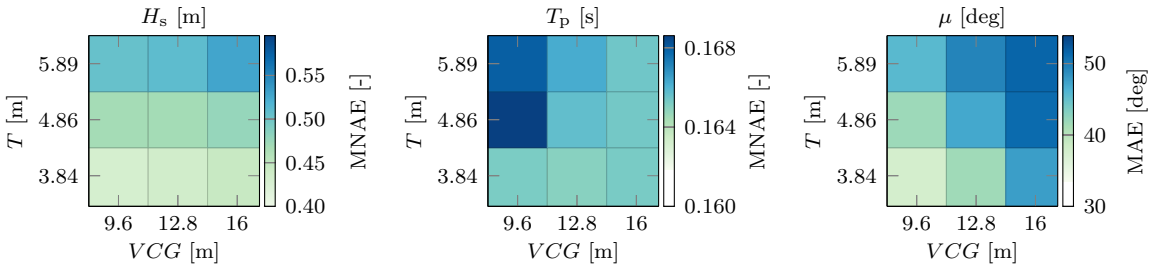

Fig. 7. Influence of draught T and vertical center of gravity VCG on the estimation accuracy of the significant wave height, peak period and relative wave direction for the measurement data. The color scale represents the magnitude of the error, with darker shades corresponding to higher error values.

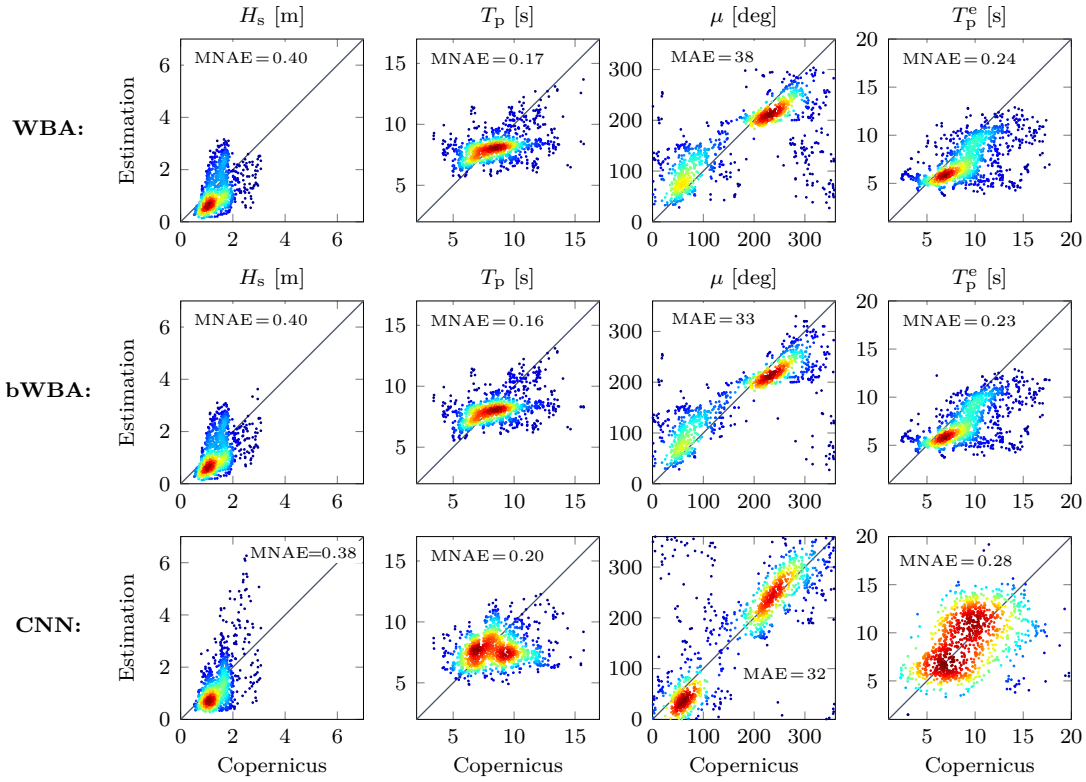

Fig. 8. Scatter density plots showing the estimations of significant wave height H_s, peak period T_p, relative wave direction μ and encounter peak period T_p^e for the WBA (top), the bWBA (middle) and the CNN (bottom) on the full-scale measurement data. Red dots indicate high and blue dots low density.

period, the WBA methods achieve similar estimation accuracies in both the absolute and encounter frequency domain. Measured by the MNAE, the CNN estimates H_s more accurately on average compared to the WBA and bWBA; however, the scatter in the estimate of the wave height increases further for higher values.

In the next step, the bWBA and the CNN were examined regarding their capabilities to reflect the energy of the ship's responses. For each sample, the relative deviation ϵ, see Eq. 10, was calculated for the zeroth-moment of heave $m_{0,3}$, roll $m_{0,4}$ and pitch acceleration $m_{0,5}$. The measured vessel response serves as ground truth, while $\hat{y}$ represents the reconstructed energy that is computed using the estimated sea state parameters and linear theory. The results are depicted in Fig. 9, next to the results from the sea state parameters obtained from Copernicus. The errors in the reference data obtained from Copernicus due to modeling assumptions or interpolation are assumed to be sufficiently small in order to determine an overall trend in this investigation. The plots on the left-hand side demonstrate that the lower the measured ship accelerations, the greater the

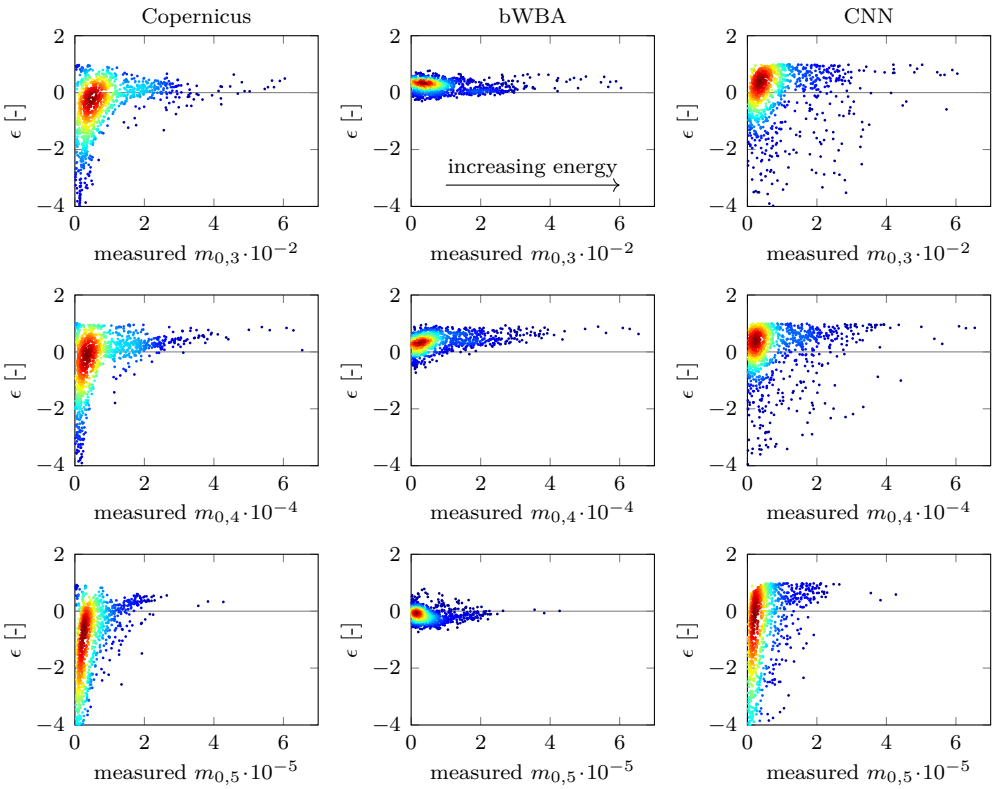

Fig. 9. Scatter density plot showing the relative error between reconstructed and measured energy of vessel responses heave ($m_{0,3}$), roll ($m_{0,4}$) and pitch accelerations ($m_{0,5}$). Results are generated using linear theory with Copernicus data (left) as well as estimations of the bWBA (middle) and the CNN (right). Red dots indicate high and blue dots low density.

relative error made by linear theory becomes. For high values of m_0, the relative deviation fluctuates around $\epsilon = 0$ for the heave and pitch acceleration, while the measured roll acceleration tends to get underestimated by linear theory. In contrast, the estimations made by the bWBA reproduces the measured ship accelerations more accurately in most cases, as the scattering significantly decreases when comparing the plots in the middle to the ones on the left-hand side. Similar to the previous observation, the accuracy regarding the roll response is worse with increasing roll energy. The results of the CNN, as depicted on the right-hand side, exhibits a similarly large scattering compared to the plots on the left-hand side. In this case, however, and no difference between the relative error for heave, pitch and roll acceleration can be observed.

5 Discussion

The investigations based on the simulation data show that the convergence of the least-squares algorithm to local minima can lead to inaccurate estimations regarding the wave energy distribution in the WBA. This can affect either solely the relative wave direction or both the wave direction and the peak period. However, the results suggest that the energy distribution in encounter frequency domain, as given by T_p^e, is captured accurately. The influence on the estimation of the significant wave height was not investigated in this study. The results demonstrate that this issue can be mitigated by constraining the least-squares algorithm to a defined range of angles, and that the case distinction regarding the wave direction works robustly. The largest difference between the CNN and the WBA methods appears in the estimation of the wave height, which is more accurate for the CNN on the simulation data set. This shows the potential advantage of the non-linear model over the linear models, as the amount of motion energy does not translate linearly into wave height.

In the next step, the methods were applied to full-scale measurement data. The study on the influence of draught T and vertical center of gravity VCG on the estimation accuracy highlights the importance

of the knowledge about the current operating conditions and therefore the RAOs in the WBA. All three methods yield similar accuracies for the sea state parameters, as measured by the MNAE and the MAE. The procedure of the bWBA and its potential improvements over the unbounded least-squares formulation were successfully validated. Analysis of the reconstructed response energies demonstrated that the bWBA has a greater capability to reproduce and capture the measured energies compared to the CNN. This allows a more comprehensible analysis of the estimations in the post-processing, whereas the results of the CNN are difficult to interpret physically due to its black-box nature. Furthermore, it was shown that the relative error of the linear theory increases as the response energy decreases, which may affect the accuracy of the WBA method. However, it should also be noted that these sea state conditions are not critical for the detection of severe sea states or large response amplitudes.
In addition to the unknown operating points of the barge, other substantial sources of error include the violation of the stationarity assumption during measurements, the simplified representation of the real sea state as a single-peak JONSWAP spectrum, measurement inaccuracies as well as discrepancies in the reference data derived from meteorological sources, which may deviate from the actual sea state due to modeling errors or local interpolation. Furthermore, the CNN was trained using data for only one Froude number for reasons of computational effort, while by the application of the WBA methods three Froude numbers are taken into account. Therefore, at this stage in the process and while the neural network has not yet attained the generalization capability regarding the operating conditions, the WBA shows an advantage over data-driven approaches, as it is currently more adaptable to varying load cases, Froude numbers, and ship geometries.

6 Conclusions

In this study, physics-based and data-driven methods for sea state estimation were implemented and tested based on simulation and measurement data. The problem of convergence to local minima in the least-squares algorithm was mitigated by constraining the WBA to a plausible range of wave directions. It should be noted here that the WBA can also be implemented using a global optimization scheme. Although the CNN, as a non-linear model, is superior to the WBA in terms of complexity, the CNN yield results that are of similar accuracy compared to the physics-based approaches. One reason for this may lie in the training data of the CNN, whose applicability is limited by the same assumptions about the operating conditions of the vessel as the WBA. In conclusion, both the bWBA and the CNN offer feasible approaches for parametric sea state estimation on the given data, with the results emphasizing the significance of known vessel-specific conditions for the WBA approach and the accuracy and representativeness of the training data for the CNN.

Future work will focus on exploring methods for tuning the RAOs to fit the current operating point during voyage, thereby reducing the associated uncertainties. The performance of the neural network could be enhanced through transfer learning, where parts of the neural network are retrained using measurement data. Under the assumption that the barge operates primarily under similar loading conditions, transfer learning could circumvent the problem of unknown operating points, as these are described through the measured data. In order to achieve capability of generalization regarding varying loading conditions, the acquisition of more data as well as further investigations of the model architecture are required. Lastly, it is emphasized that both methods can be combined in a hybrid model in which the disadvantages of one method are complemented by the advantages of the other.

Acknowledgments

Measurement data was obtained from RetroLadung, which was funded within the framework program "Maritime Technologies of the Next Generation" by the German Federal Ministry of Economic Affairs and Energy. The project funding was administered by Projektträger Jülich under grant number 03SX484C. Furthermore, this study has been conducted using E.U. Copernicus Marine Service Information; DOI: 10.48670/moi-00022.

References

1. Bačkalov, I., Bulian, G., Rosén, A., Shigunov, V., Themelis, N.: Improvement of ship stability and safety in intact condition through operational measures: challenges and opportunities. Ocean Engineering 120, 353-361 (2016). https://doi.org/10.1016/j.oceaneng.2016.02.011.
2. Takashima K., Mezaoui B., Shoji R.: On the fuel saving operation for coastal merchant ships using weather routing. TransNav, the International Journal on Marine Navigation and Safety of Sea Transportation 3(4), 401-406 (2009). https://doi.org/10.1201/9780203869345.ch75.
3. Tannuri, E.A., Sparano, J.V., Simos, A.N., Da Cruz, J.J.: Estimating directional wave spectrum based on stationary ship motion measurements. Applied Ocean Research 25(5), 243-261 (2003). https://doi.org/10.1016/j.apor.2004.01.003.
4. Iseki, T., Ohtsu, K.: Bayesian estimation of directional wave spectra based on ship motions. Control Engineering Practice 8(2), 215-219 (2000). https://doi.org/10.1016/S0967-0661(99)00156-2.
5. Nielsen, U.D.: Estimations of on-site directional wave spectra from measured ship responses. Marine Structures 19(1), 33-69 (2006). https://doi.org/10.1016/j.marstruc.2006.06.001.
6. Nielsen, U.D.: A concise account of techniques available for shipboard sea state estimation. Ocean Engineering 129, 352-362 (2017). https://doi.org/10.1016/j.oceaneng.2016.11.035.
7. Pascoal, R., Perera, L.P., Guedes Soares C.: Estimation of directional sea spectra from ship motions in sea trials. Ocean Engineering 132, 126-137 (2017). https://doi.org/10.1016/j.oceaneng.2017.01.020.
8. Nielsen, U.D.: Response-based estimation of sea state parameters — influence of filtering. Ocean Engineering 34(13), 1797-1810 (2007). https://doi.org/10.1016/j.oceaneng.2007.03.002.
9. Iseki, T., Nielsen, U.D.: Study on short-term variability of ship responses in waves. The Journal of Japan Institute of Navigation 132, 51-57 (2015). https://doi.org/10.9749/jin.132.51
10. Mittendorf, M., Nielsen, U.D., Bingham, H.B., Storhaug G.: Sea state identification using machine learning—A comparative study based on in-service data from a container vessel. Marine Structures 85 (2022). https://doi.org/10.1016/j.marstruc.2022.103274
11. Mittendorf, M., Nielsen, U.D., Bingham, H.B., Storhaug G.: On the determination of the relative wave direction based on measured ship responses using deep multi-task learning. In: Proceeding HIPER 2022, pp. 96-106.
12. Kawai, T., Kawamura, Y., Okada, T., Taiga, M., Xi, C.: Sea state estimation using monitoring data by convolutional neural network (CNN). Journal of Marine Science and Technology 26, 947–962 (2021). https://doi.org/10.1007/s00773-020-00785-8.
13. Han, P., Li, G., Cheng, X., Skjong, S., Zhang, H.: An uncertainty-aware hybrid approach for sea state estimation using ship motion responses. IEEE Transactions on Industrial Informatics 18(2), 891-900 (2022). https://doi.org/10.1109/TII.2021.3073462.
14. Nielsen, U.D., Mittendorf, M., Shao, Y., Storhaug, G.: Wave spectrum estimation conditioned on machine learning-based output using the wave buoy analogy. Marine Structures 91. 2023. https://doi.org/10.1016/j.marstruc.2023.103470.
15. Nielsen, U.D.: The wave buoy analogy — estimating high-frequency wave excitations. Applied Ocean Research 30(2). 100-106 (2008). https://doi.org/10.1016/j.apor.2008.07.002.
16. Brodtkorb, A.H., Nielsen, U.D.: Automatic sea state estimation with online trust measure based on ship response measurements. Control Engineering Practice 130. 2023. https://doi.org/10.1016/j.conengprac.2022.105375.
17. Rosenblatt, F.: The perceptron: A probabilistic model for information storage and organization in the brain. Psychological Review 65(6), 386–408 (1958). https://doi.org/10.1037/h0042519.
18. Goodfellow, I., Bengio, Y., Courville, A.: Deep Learning. MIT Press (2016). http://www.deeplearningbook.org.
19. Global Ocean Waves Reanalysis. E.U. Copernicus Marine Service Information (CMEMS). Marine Data Store (MDS). Accessed on 08/01/2022. https://doi.org/10.48670/moi-00022.
20. Cummins, W.E.: The impulse response function and ship motions. Schiffstechnik 47, 101-109 (1962). https://dome.mit.edu/handle/1721.3/49049.
21. Wermbter, M., Abdel-Maksoud, M.: Calculation of ship motions in steep waves with restoring and Froude-Krylov forces on an adaptive panel mesh with Gauss and analytic integration methods. Journal of Hydrodynamics 36, 275–289 (2024). https://doi.org/10.1007/s42241-024-0026-6.
22. Söding, H.: Global Seaway Statistics. TU Hamburg-Harburg Schriftenreihe Schiffbau 610 (2001).
23. Han, X., Sævik, S., Leira, B.J.: A sensitivity study of vessel hydrodynamic model parameters. In: Proceedings of the ASME 2020 39th International Conference on Ocean, Offshore and Arctic Engineering, vol. 1. 2020. https://doi.org/10.1115/OMAE2020-19039.

A Appendix - Hyperparameter Study

First, an independent test set holding 800 samples was extracted from the data. The remaining 3200 data samples were split into a train and validation set following the four-fold cross-validation method. The early-stopping function was applied and the weights and loss values of the best model on the validation set was restored. Table 2 presents the resulting losses in terms of mean and standard deviation for the four runs carried out. The variations of hyperparameters include the number of kernels in the convolutional layers and the number of neurons in the fully-connected layers. The best model was selected based on the lowest loss on the validation set. Next, the resulting architecture was investigated regarding under- and overfitting. The train and validation set were merged into a new train set and the model was tested using the data from the test set. The results of varying the train set size is depicted in Figure 10a. The model trained on 3200 data samples was set as final. The corresponding loss curves over the epochs are shown in Figure 10b.

Table 2. The loss is given as mean and standard deviation for the train and test set.

conv. layers		fully-conn. layers.		loss	
# kernels	kernel size	# neurons	# train. par.	train	val
$[16, 32, 64, 128]$	3	$[32, 64]$	30004	0.00469 ± 0.00058	0.0130 ± 0.00323
		$[64, 128]$	574932	0.00367 ± 0.00104	0.0112 ± 0.00234
		$[128, 256]$	1133076	0.00251 ± 0.00042	0.0115 ± 0.00283
$[32, 64, 128, 256]$	3	$[32, 64]$	665924	0.00303 ± 0.00024	0.01232 ± 0.0034
		$[64, 128]$	1205092	0.00214 ± 0.00058	0.01083 ± 0.0008
		$[128, 256]$	2295716	0.00187 ± 0.00023	0.01283 ± 0.0006

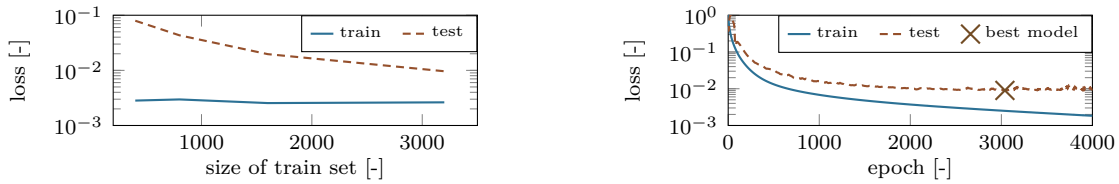

(a) Variation of the train set size

(b) Learning curves

Fig. 10. Left: Loss values of the train and test set over the train set size. Right: Loss values of the train and test set for a train set size of 3200. The best model regarding the loss on the test set is marked.